Science Translational Medicine
AAAS

stm.sciencemag.org/cgi/content/full/11/504/eaau4972/DC1

Supplementary Materials for

Targeting pyrimidine synthesis accentuates molecular therapy response in glioblastoma stem cells

Xiuxing Wang, Kailin Yang, Qiulian Wu, Leo J. Y. Kim, Andrew R. Morton, Ryan C. Gimple, Briana C. Prager, Yu Shi, Wenchao Zhou, Shruti Bhargava, Zhe Zhu, Li Jiang, Weiwei Tao, Zhixin Qiu, Linjie Zhao, Guoxing Zhang, Xiqing Li, Sameer Agnihotri, Paul S. Mischel, Stephen C. Mack, Shideng Bao, Jeremy N. Rich*

*Corresponding author. Email: drjeremyrich@gmail.com

Published 7 August 2019, *Sci. Transl. Med.* **11**, eaau4972 (2019)
DOI: 10.1126/scitranslmed.aau4972

The PDF file includes:

Other Supplementary Material for this manuscript includes the following:

(available at stm.sciencemag.org/cgi/content/full/11/504/eaau4972/DC1)

Data file S1. Individual subject-level data (Excel file).

Materials and Methods

Chromatin immunoprecipitation with sequencing (ChIP-seq)

4×10^6 cells of GSCs or DGCs were first flash frozen. 5-10 mg of cell lysate from each specimen was mixed with 5 mg histone H3K27ac antibody (Active Motif #39155). Chromatin immunoprecipitation was performed using EZ-ChIP chromatin immunoprecipitation kit (EMD Millipore). Heating for 6 hours at 65 °C was preformed to reverse crosslinking, followed with digestion using proteinase K. Enriched DNA was quantified using Picogreen (Invitrogen). ChIP libraries were then amplified with barcode using ThruPLEX DNA-seq library preparation kit (Rubicon Genomics). 1.0% agarose gel was used to select DNA fragments less than 1 kb, followed by 100 bp single-end sequencing performed with Hi-Seq 2000 (Illumina).

Whole-exome sequencing variant discovery

The exome paired-end reads were aligned to reference genome hg19 with BWA-MEM version 0.7.12. BAM files were processed using SAMtools and PCR duplicates were removed with PicardTools (http://broadinstitute.github.io/picard/). The Genome Analysis Toolkit (GATK) version 3.8 was used to identify variants in accordance with their best practices. SNPeff was used to find non-synonymous and splice site variants that may have an effect on protein sequence or structure. Potential pathogenic variants were identified in commonly mutated glioblastoma genes (*20*), making sure the variants were not found at any allelic frequency in the Exome Aggregation Consortium release 1 (*61*) and 1000 Genomes Project (*62*). CopywriteR (*63*) was used to find focal copy number variants in common glioblastoma oncogenes and tumor suppressors.

Plasmids and gene knockdown

Plasmids expressing shRNAs targeting human DHODH (TRCN0000025868, TRCN0000025839), human CAD (TRCN0000045910, TRCN0000045908), and a control shRNA with no targets in both human and mouse genomes (shCONT: SHC002) were purchased from Sigma-Aldrich. ShRNAs with non-overlapping sequences that had the best relative knockdown efficiency were used for all experiments. Lentiviral particles were generated in 293FT cells in Neurobasal complete medium (Life Technologies) with co-transfection with the packaging vectors pCMV-dR8.2 dvpr and pCI-VSVG (Addgene) using standard calcium phosphate transfection method.

Proliferation and neurosphere formation assay

Cell-Titer Glow (Promega) was used to determine cell proliferation rate. Data points were normalized to that of day 0 and presented as mean ± SEM. In vitro limiting dilution assay was used to measure neurosphere formation, as previously described (*16, 19*). Briefly, decreasing numbers of cells per well (50, 20, 10, 5, and 1) were plated into 96-well plates. Seven days after plating, the presence and number of neurospheres in each well were recorded. The results were calculated using extreme limiting dilution analysis, as previously described (*16, 19*).

Compounds

The following inhibitors (with the main molecular target, manufacturer, and catalog number in parenthesis) were used in this study: U0126 (MEK, Cell Signaling Technology #9903S) (*64*), GSK1120212/trametinib (MEK, Cayman Chemical #871700-17-3) (*65*), BKM120/buparlisib (PI3K, MedChem Express #HY-70063) (*66*), LY294002 (PI3K, Cell Signaling Technology #9901S) (*67*), rapamycin (mTOR, Cell Signaling Technology #9904S) (*68*), lapatinib (EGFR, MedChem Express #HY-50898) (*69*), gefitinib (EGFR, Sigma #SML1657) (*70*), and teriflunomide (DHODH, MedChem Express #HY-15405) (*71*).

Western blotting

RIPA buffer was used to lyse cells (50 mM Tris-HCl, pH 7.5; 150 mM NaCl; 0.5% NP-40; 50 mM NaF with protease inhibitors), followed by incubation on ice for 30 minutes. Lysates were then centrifuged at 4°C for 10 minutes with the speed of 14,000 rpm, and the pellets were discarded. Bradford assay (Bio-Rad) was used to determine protein concentration, with equal amounts of protein specimens mixed and boiled with SDS Laemmli loading buffer. Electrophoresis was performed using NuPAGE Bis-Tris gels (Life Technologies), followed by transfer onto PVDF membranes (Millipore). TBST supplemented with 5% non-fat dry milk was used for blocking. Blotting with primary antibody was performed at 4 °C for 16 hours. The following antibodies were used: total CAD (Cell Signaling Technology #11933), phosphorylated-CAD^{S1859} (Cell Signaling Technology #67235), phosphorylated-CAD^{T456} (Santa Cruz Biotechnology #sc-12964), DHODH (Abcam #ab174288), SOX2 (R&D Systems #AF2018), total ERK (Cell Signaling Technoogy #9102), phosphorylated-ERK (Cell Signaling Technology #9101), total AKT (Cell Signaling Technology #4691), phosphorylated-AKT^{S473} (Cell Signaling Technology #9271), total S6 (Cell Signaling Technology #2217), phosphorylated-S6$^{S235/236}$ (Cell Signaling Technology #4858), total p70 S6K (Cell Signaling Technology #2708), histone H3K27me3 (Active Motif #39155), and α-Tubulin (Sigma #T9026). Quantification of protein expression was performed using ImageJ (*72*), and α-Tubulin was used as the loading control for normalization.

Mass spectrometry

Targeted mass spectrometry was used to determine the concentrations of pyrimidine synthesis intermediates. Pure specimens of CTP, UMP, and dihydroorotate were purchased from Sigma. All solvents were purchased from Fisher Scientific. Cells were dried, and cell lysates were reconstituted with 180 µl of water added with 20 µl of internal standard (50 µM Adenosine 5'-Monophosphate-$^{13}C_5$). After vortexing for 60 seconds, the reconstituted samples were centrifuged at 12,000 rpm at 4 °C for 10 min.

The supernatant was the subjected to analysis for LC/MS/MS, using Waters 2690 Module HPLC system directly interfaced with triple-quadrupole mass spectrometer. Peak area in LC/MS/MS chromatogram was generated using QuanLynx attached with Masslynx software for each metabolite and internal standard. The calibration curve of internal standard was then used to quantify each metabolite in the cell lysates.

In vivo tumorigenesis

All in vivo tumorigenesis experiments in mice were performed in according to an animal protocol approved by the Institutional Animal Care and Use Committee at University of California, San Diego. Viable GSCs were quantified and intracranially injected into NSG mice (NOD.Cg-Prkdcscid Il2rgtm1Wjl/SzJ, The Jackson Laboratory). For knockdown experiments, GSCs were first infected with lentiviruses expressing the respective shRNA for 36 hours prior to injection to mice. For inhibitor treatment, mice were treated with control DMSO vehicle, teriflunomide (50 mg/kg every 2 days), BKM120 (50 mg/kg every 2 days), lapatinib (50 mg/kg every 2 days), or respective combinations until the end point. Mice were then maintained until apparent neurological signs were observed, when they would be sacrificed for further analysis. Brain harvesting was performed followed by fixation in 4% formaldehyde, cryopreservation in 30% sucrose, and then cryosection. Hematoxylin and eosin staining was performed on brain sections for histological analysis.

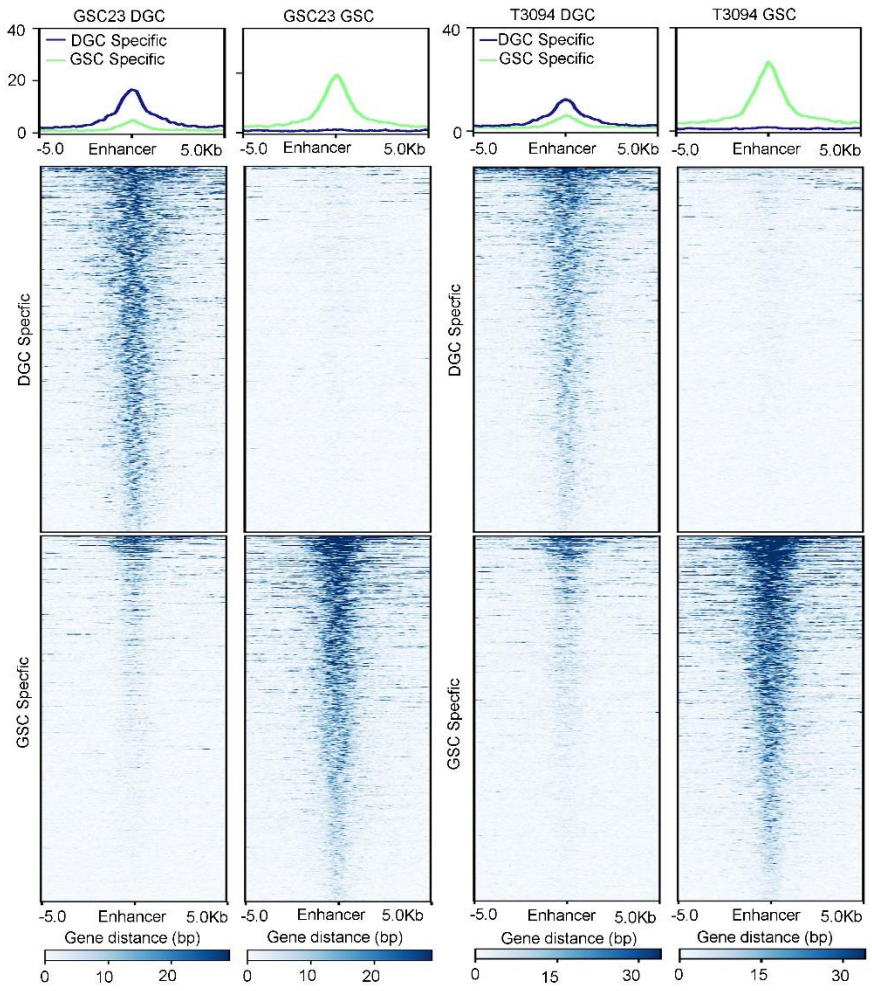

Fig. S1. Identification of differential enhancer activation between GSCs and DGCs. Patient-derived GSCs (glioblastoma stem cells; GSC23 and T3094) were cultured under serum-free conditions to maintain their GSC state or induced into differentiated glioblastoma cells (DGCs), then subjected to histone 3 lysine 27 acetyl chromatin immunoprecipitation followed by deep sequencing (H3K27ac ChIP-seq). Comparative coverage plots between matched GSCs and DGCs illustrate the specific enhancers in GSC23 (left) and T3094 (right). Heat maps are shown to depict H3K27ac signal, normalized to read depth, for ±5 kb surrounding enhancer peaks. Color scale indicates reads per kilobase per million mapped reads (RPKM). The y-axis is normalized H3K27ac read depth (RPKM).

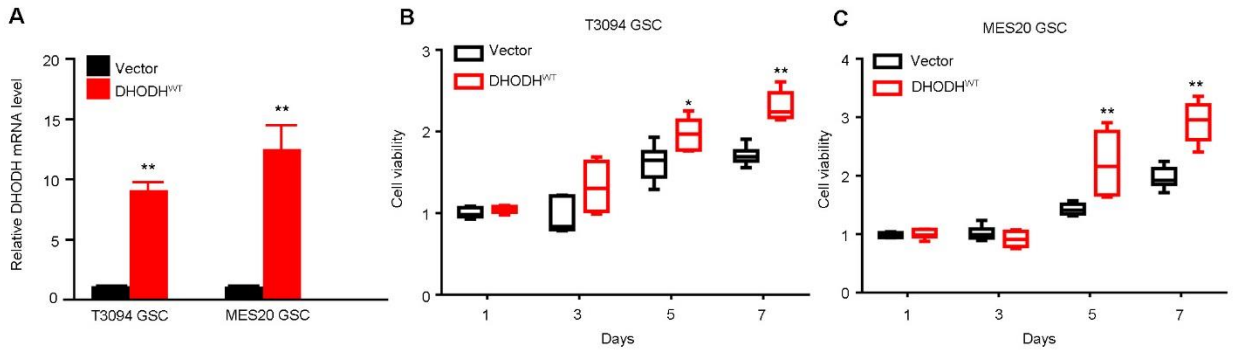

Fig. S2. DHODH promotes GSC growth. (**A**) Quantitative RT-PCR assessment of DHODH mRNA levels in T3094 and MES20 GSCs transduced with either empty vector (Vector) or wild-type DHODH ($DHODH^{WT}$) (n = 3 independent experiments per group; ** $P < 0.01$ using two-sided Student's t-test). (**B**) and (**C**) T3094 and MES20 GSCs were transduced with vector control or $DHODH^{WT}$. Cell growth was quantified by CellTiter-Glo over a time course. (n = 6 independent experiments per group; * $P < 0.05$, ** $P < 0.01$ using two-sided Student's t-test at each time point).

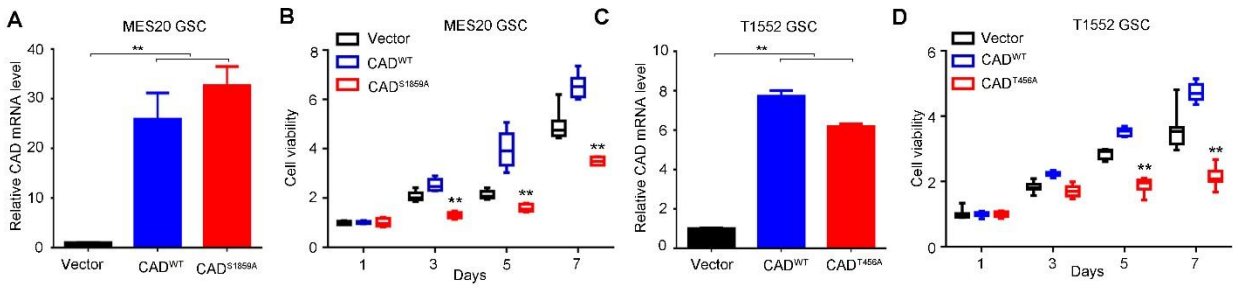

Fig. S3. CAD^{S1859} and CAD^{T456} are important for GSC proliferation. (**A**) Quantitative RT-PCR assessment of CAD mRNA levels in PTEN-deleted MES20 GSCs overexpressing empty vector (Vector), wild-type CAD (CAD^{WT}), or CAD^{S1859A} (n = 3 independent experiments per group; ** P < 0.01 using one-way ANOVA). (**B**) MES20 GSCs were transduced with a vector control, CAD^{WT}, or CAD^{S1859A}. Effects on proliferation were measured by CellTiter-Glo assay (n = 6 independent experiments per group; ** P < 0.01 using one-way ANOVA). (**C**) T1552 GSCs harboring EGFR amplifications were transduced with empty vector (Vector), CAD^{WT}, or CAD^{T456A}. CAD mRNA levels were measured by quantitative RT-PCR (n = 3 independent experiments per group; ** P < 0.01 using one-way ANOVA). (**D**) Overexpressing CAD^{T456A} decreased growth of T1552 GSCs in comparison to empty vector or CAD^{WT}, as measured by CellTiter-Glo assay (n = 6 independent experiments per group; ** P < 0.01 using one-way ANOVA).

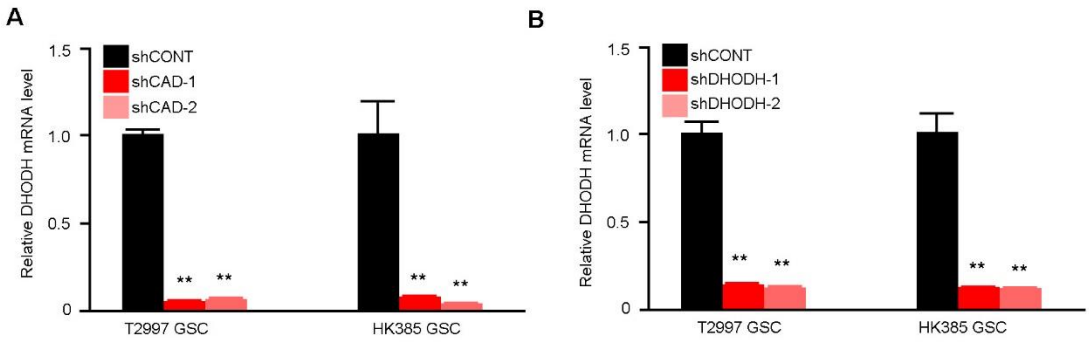

Fig. S4. Validation of knockdown efficacy of shRNAs directed against CAD. (**A**) and (**B**) Quantitative RT-PCR assessment of CAD and DHODH mRNA expressions in GSC23 and T456 GSCs transduced with shCONT, shCAD-1, or shCAD-2 (n = 3 independent experiments per group; ** $P < 0.01$ using one-way ANOVA).

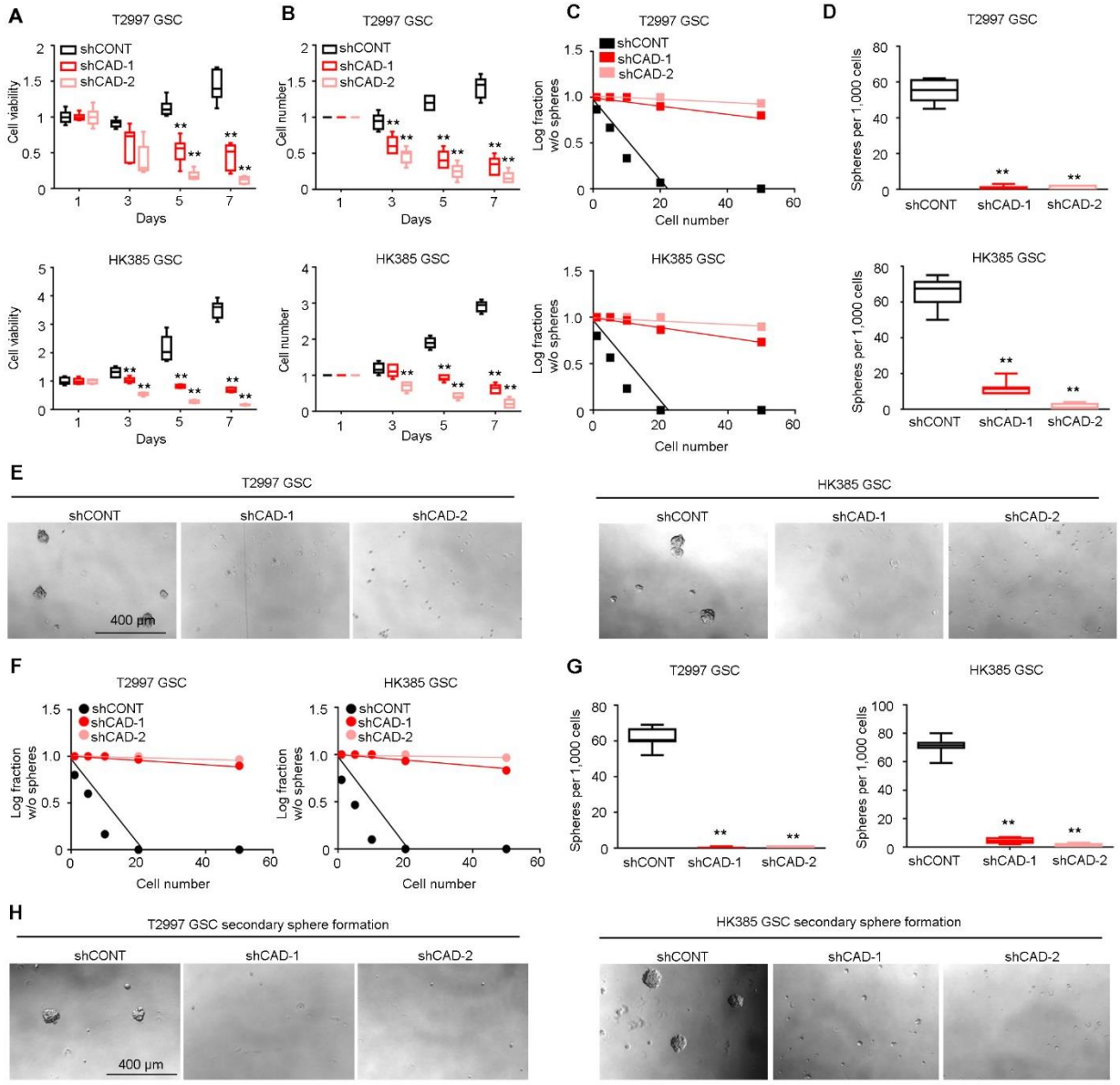

Fig. S5. CAD regulates primary GSC growth and self-renewal. (**A**) T2997 and HK385 GSCs were transduced with one of two independent shRNAs targeting CAD (shCAD-1 or shCAD-2) or a non-targeting control shRNA (shCONT). Cell growth was measured by the CellTiter-Glo assay (n = 6 independent experiments per group; ** $P < 0.01$ using one-way ANOVA). (**B**) Cell growth, as measured by direct cell number count, in T2997 and HK 385 GSCs expressing shCONT, shCAD-1, or shCAD-2 (n = 6 independent experiments per group; ** $P < 0.01$ using one-way ANOVA). (**C**) Sphere formation using an extreme limiting dilution assay (ELDA) in T2997 and HK 385 GSCs expressing shCONT, shCAD-1, or shCAD-2 (n =

10 independent experiments per group). (**D**) Number of spheres formed per 1,000 cells seeded in T2997 and HK 385 GSCs expressing shCONT, shCAD-1, or shCAD-2 (n = 10 independent experiments per group; ** $P < 0.01$ using one-way ANOVA). (**E**) Representative images of neurospheres derived from T2997 and HK385 GSCs transduced with shCONT, shCAD-1, or shCAD-2. (**F**) Secondary sphere formation using an ELDA in T2997 and HK 385 GSCs expressing shCONT, shCAD-1, or shCAD-2 (n = 10 independent experiments per group). (**G**) Number of spheres formed using a secondary assay per 1,000 cells seeded in T2997 and HK 385 GSCs expressing shCONT, shCAD-1, or shCAD-2 (n = 10 independent experiments per group; ** $P < 0.01$ using one-way ANOVA). (**H**) Representative images of secondary neurospheres derived from T2997 and HK385 GSCs transduced with shCONT, shCAD-1 or shCAD-2. Scale bar, 100 µm. Each image is representative of at least 5 similar experiments.

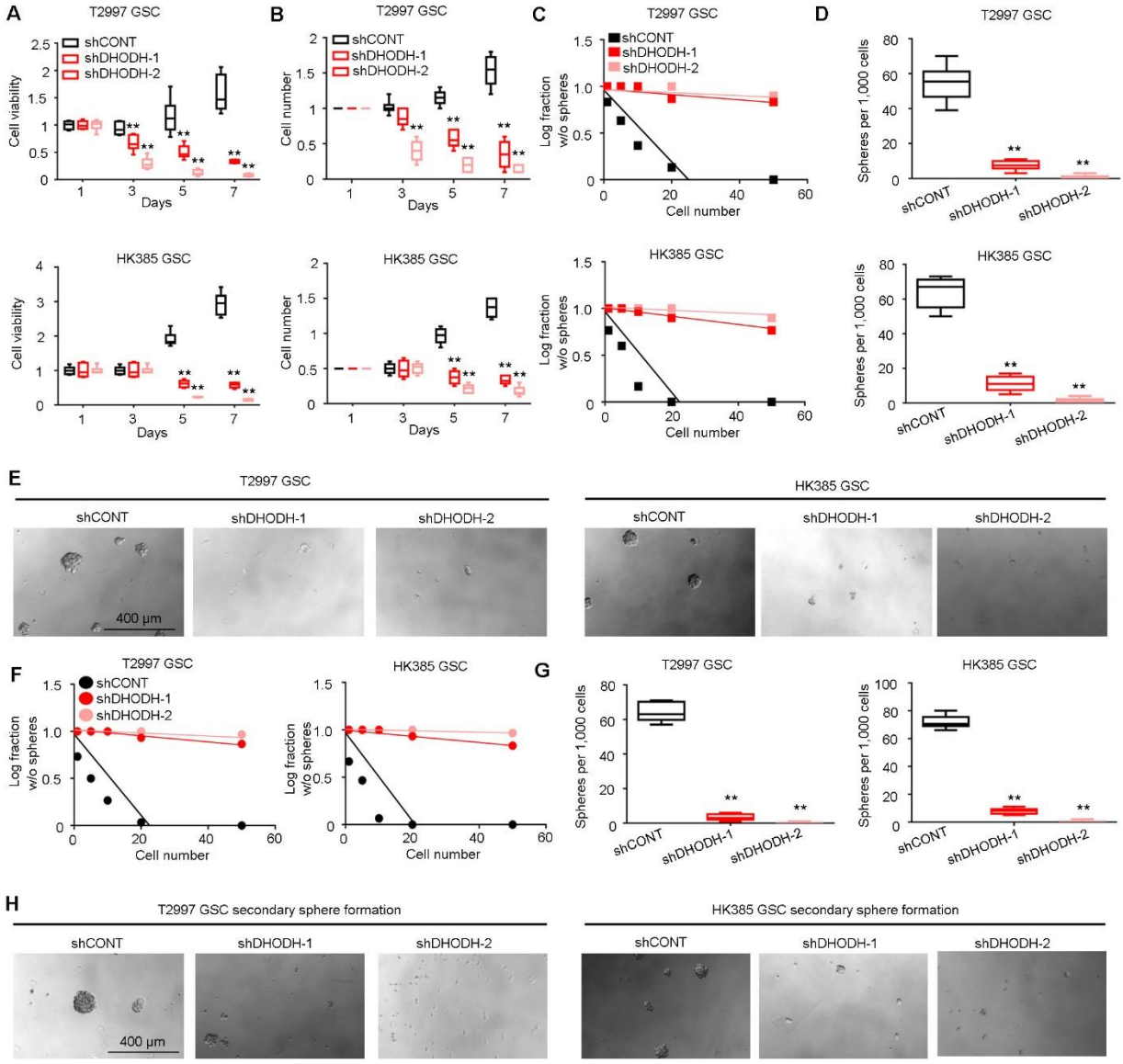

Fig. S6. DHODH regulates primary GSC growth and self-renewal. (**A**) T2997 and HK385 GSCs were transduced with one of two independent shRNAs targeting DHODH (shDHODH-1 or shDHODH-2) or a non-targeting control shRNA (shCONT). Proliferation was measured by CellTiter-Glo assay (n = 6 independent experiments per group; ** P < 0.01 using one-way ANOVA). (**B**) Cell growth, as measured by direct cell number count, in T2997 and HK 385 GSCs expressing shCONT, shDHODH-1, or shDHODH-2 (n = 6 independent experiments per group; ** P < 0.01 using one-way ANOVA). (**C**) Sphere formation using an extreme limiting dilution assay (ELDA) in T2997 and HK 385 GSCs expressing shDHODH-1,

shDHODH-2, or shCONT (n = 10 independent experiments per group). (**D**) Number of spheres formed per 1,000 cells seeded in T2997 and HK 385 GSCs expressing shCONT, shDHODH-1, or shDHODH-2 (n = 10 independent experiments per group; ** P < 0.01 using one-way ANOVA). (**E**) Representative images of neurospheres derived from T2997 and HK385 GSCs transduced with shCONT, shDHODH-1 or shDHODH-2. (**F**) Secondary sphere formation using an ELDA in T2997 and HK385 GSCs transduced with shCONT, shDHODH-1 or shDHODH-2 (n = 10 independent experiments per group). (**G**) Number of spheres formed in secondary assay per 1,000 cells seeded in T2997 and HK385 GSCs transduced with shCONT, shDHODH-1 or shDHODH-2 (n = 10 independent experiments per group; ** P < 0.01 using one-way ANOVA). (**H**) Representative images of secondary neurospheres derived from T2997 and HK385 GSCs transduced with shCONT, shDHODH-1 or shDHODH-2. Scale bar, 100 µm. Each image is representative of at least 5 similar experiments.

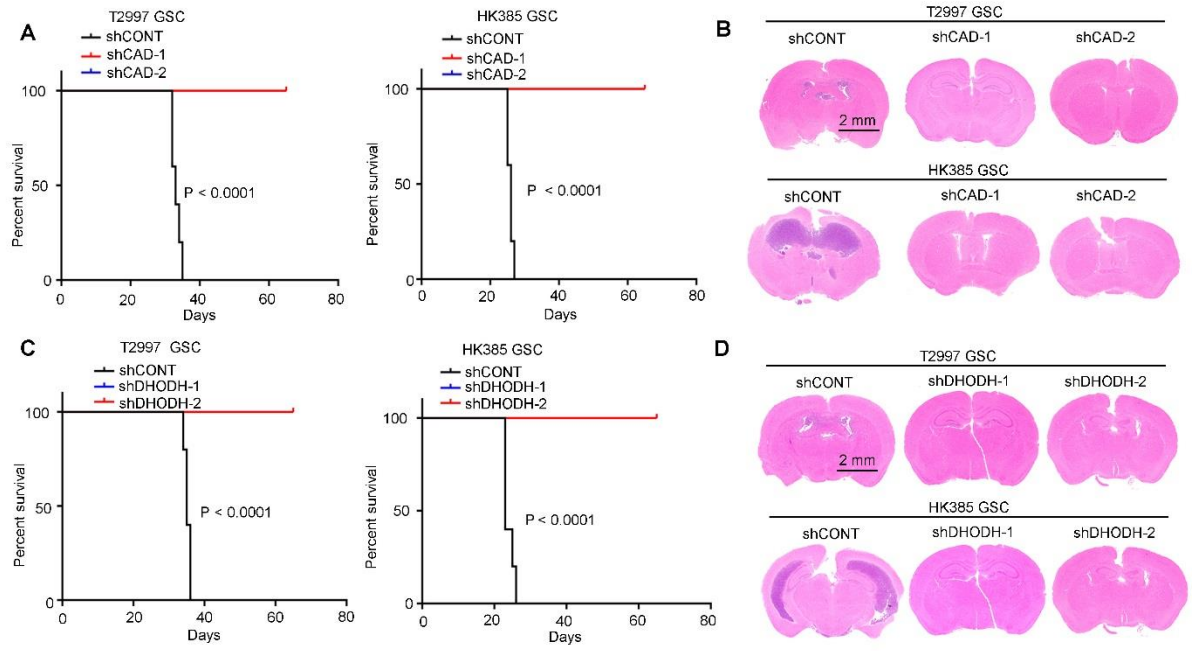

Fig. S7. CAD and DHODH are essential for primary GSC maintenance. (**A**) Kaplan-Meier survival curves of immunocompromised mice bearing intracranial T2997 or HK385 GSCs transduced with either a control shRNA (shCONT) or one of two shRNAs targeting CAD (shCAD-1 or shCAD-2) (n = 5 independent experiments per group; P < 0.0001 using log-rank test). (**B**) Representative images of hematoxylin and eosin stained sections of mouse brains collected on day 20 after transplantation of HK385 or T2997 GSCs expressing shCONT, shCAD-1 or shCAD-2. Scale bar, 2 mm. (**C**) Kaplan-Meier survival curves of immunocompromised mice bearing intracranial T2997 or HK385 GSCs expressing shCONT or one of two shRNAs targeting DHODH (shDHODH-1 or shDHODH-2) (n = 5 independent experiments per group; P < 0.0001 using log-rank test). (**D**) Representative images of hematoxylin and eosin stained sections of mouse brains collected on day 20 after transplantation of T2997 or HK385 GSCs expressing shCONT, shDHODH-1 or shDHODH-2. Scale bar, 2 mm.

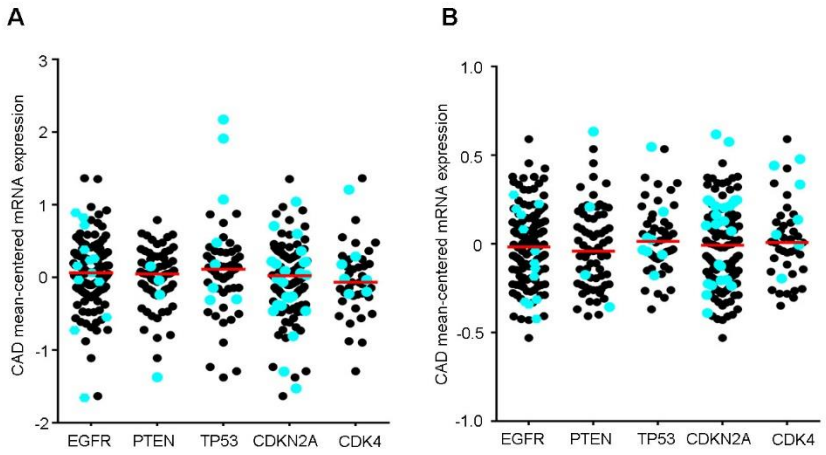

Fig. S8. Expression of pyrimidine synthesis genes remains unchanged across glioblastoma specimens harboring different driver mutations. (**A**) and (**B**) Overall mRNA expressions of CAD (**A**) and DHODH (**B**) across TCGA glioblastoma specimens with different gene mutations/alterations, including EGFR, PTEN, TP53, CDKN2A, or CDK4.

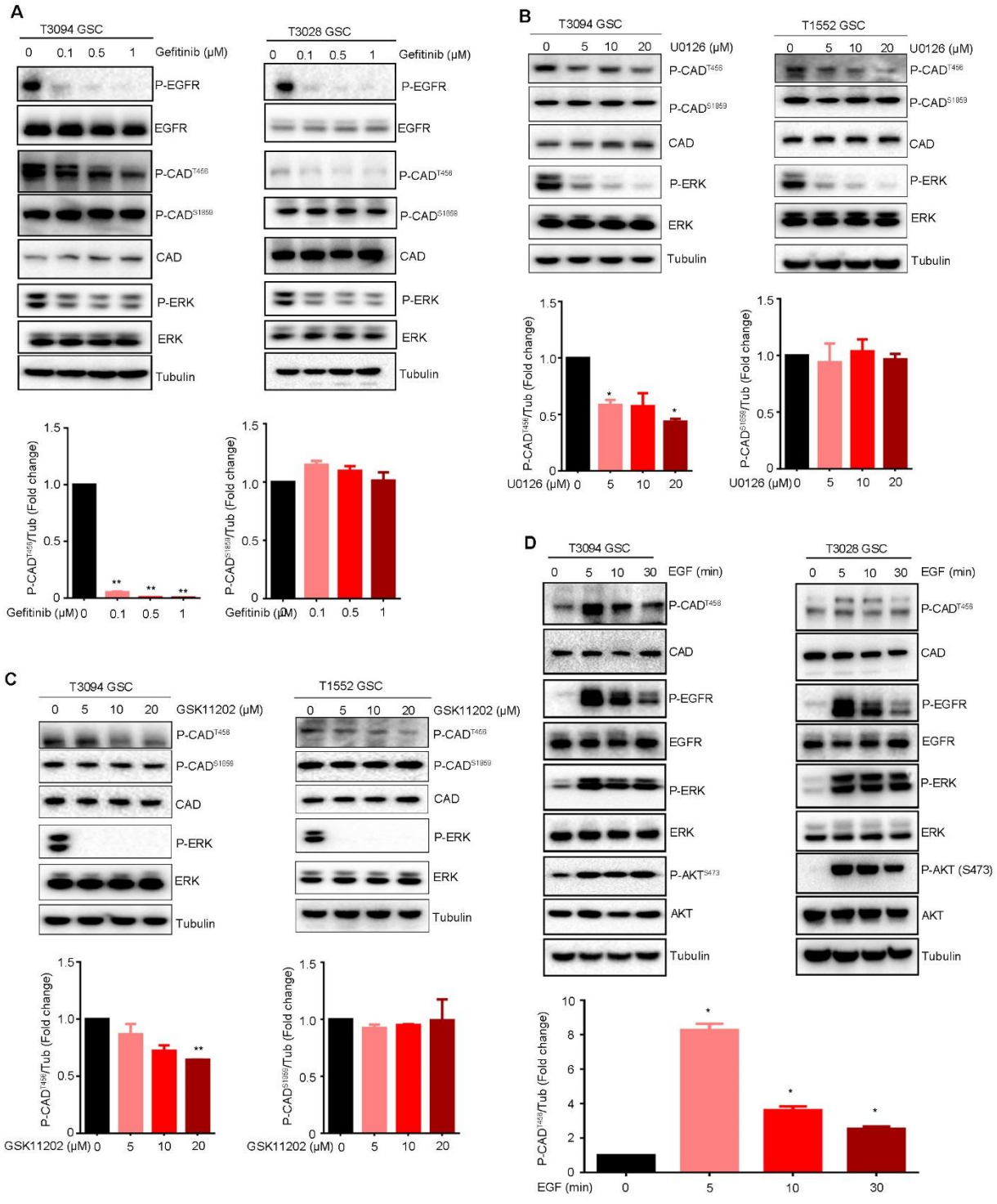

Fig. S9. EGFR regulates CAD^{T456} phosphorylation through the MAPK-ERK pathway. (**A**) Immunoblot assessment of phosphorylated-CAD^{S1859}, phosphorylated-CAD^{T456} and total CAD protein levels after treatment with the EGFR inhibitor gefitinib (0.1, 0.5, and 1 μM) for 48 hours in T3094 and T3028 GSCs.

Normalized quantifications with Tubulin as control were performed for phosphorylated-CAD^{S1859} and phosphorylated-CAD^{T456} (n = 2 biological replicates; ** P < 0.01 using one-way ANOVA). (**B**) Immunoblot assessment of phosphorylated-CAD^{S1859}, phosphorylated-CAD^{T456}, total CAD, phosphorylated-ERK and total ERK levels after treatment with the MEK inhibitor U0126 (5, 10, and 20 μM) for 48 hours in T3094 and T1552 GSCs. Normalized quantifications with Tubulin as control were performed for phosphorylated-CAD^{S1859} and phosphorylated-CAD^{T456} (n = 2 biological replicates; * P < 0.05 using one-way ANOVA). (**C**) Immunoblot assessment of phosphorylated-CAD^{S1859}, phosphorylated-CAD^{T456}, total CAD, phosphorylated-ERK and total ERK levels after treatment with the MEK inhibitor GSK1120212 (1, 5, and 10 μM) for 48 hours in T3094 and T1552 GSCs. Normalized quantifications with Tubulin as control were performed for phosphorylated-CAD^{S1859} and phosphorylated-CAD^{T456} (n = 2 biological replicates; ** P < 0.01 using one-way ANOVA). (**D**) GSCs (T3094 and T3028) were treated with EGF (100 ng/ml) over a 30 minute time course. Amounts of phosphorylated-CAD^{T456}, total CAD, phosphorylated-EGFR, total EGFR, phosphorylated-ERK, total ERK, phosphorylated-AKT^{S473} and total AKT were assessed by immunoblot. Normalized quantifications with Tubulin as control were performed for phosphorylated-CAD^{T456} (n = 2 biological replicates; * P < 0.05 using one-way ANOVA).

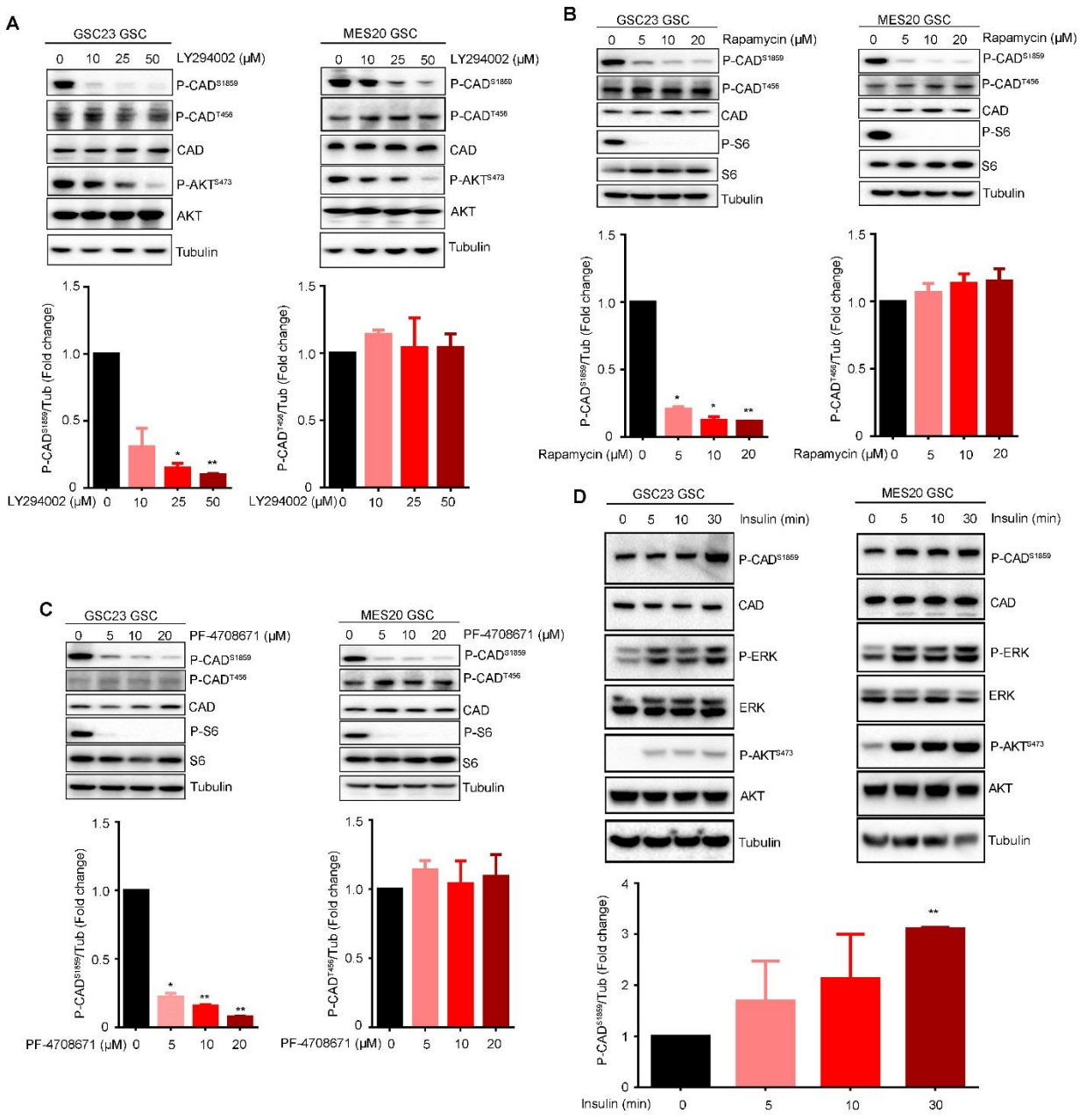

Fig. S10. PTEN deletion promotes CAD^{S1859} phosphorylation through the PI3K-AKT pathway. (**A**) Immunoblot assessment of phosphorylated-CAD^{S1859}, phosphorylated-CAD^{T456}, total CAD, phosphorylated-AKT^{S473} and total AKT levels after treatment with the PI3K inhibitor LY294002 (10, 25, and 50 μM) for 48 hours in GSC23 and MES20 GSCs. Normalized quantifications with Tubulin as control were performed for phosphorylated-CAD^{S1859} and phosphorylated-CAD^{T456} (n = 2 biological replicates; *

P < 0.05, ** P<0.01 using one-way ANOVA). (**B**) Immunoblot assessment of phosphorylated-CAD^{S1859}, phosphorylated-CAD^{T456}, total CAD, phosphorylated-S6$^{S235/236}$ and total S6 protein levels after treatment with the mTOR inhibitor, rapamycin (5, 10, and 20 μM) for 48 hours in GSC23 and MES20 GSCs. Normalized quantifications with Tubulin as control were performed for phosphorylated-CAD^{S1859} and phosphorylated-CAD^{T456} (n = 2 biological replicates; * P<0.05, ** P<0.01 using one-way ANOVA). (**C**) Immunoblot assessment of phosphorylated-CAD^{S1859}, phosphorylated-CAD^{T456}, total CAD, phosphorylated-S6$^{S235/236}$ and total S6 protein levels after treatment with the S6K1 inhibitor, PF-4708671 (5, 10, and 20 μM) for 48 hours in GSC23 and MES20 GSCs. Normalized quantifications with Tubulin as control were performed for phosphorylated-CAD^{S1859} and phosphorylated-CAD^{T456} (n = 2 biological replicates; * P<0.05, ** P<0.01 using one-way ANOVA). (**D**) GSCs (GSC23 and MES20) were treated with insulin (1 μM) over a 30-min time course. Amounts of phosphorylated-CAD^{S1859}, total CAD, phosphorylated-ERK, total ERK, phosphorylated-AKT^{S473} and total AKT were assessed by immunoblot. Normalized quantifications with Tubulin as control were performed for phosphorylated-CAD^{S1859} (n = 2 biological replicates; ** P<0.01 using one-way ANOVA).

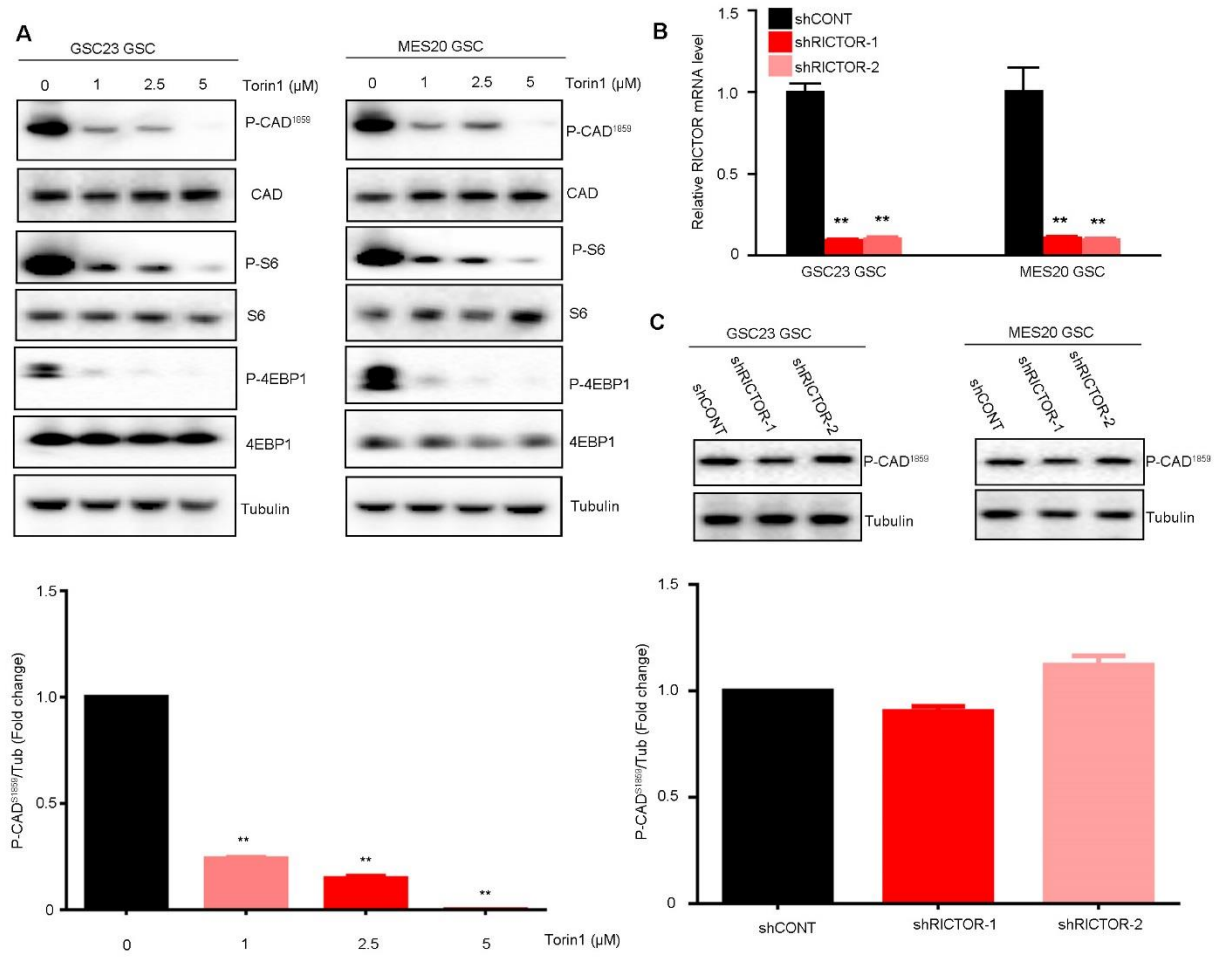

Fig. S11. PTEN deletion promotes CAD^{S1859} phosphorylation through the PI3K-AKT-TORC1 but not the TORC2 pathway. (**A**) Immunoblot assessment of phosphorylated-CAD^{S1859}, phosphorylated-AKT^{S473}, total AKT, phosphorylated-S6, total S6, phosphorylated-4EBP1 and total 4EBP1levels after treatment with the PI3K inhibitor LY294002 (10, 25, and 50 μM) for 48 hours in GSC23 and MES20 GSCs. Normalized quantifications with Tubulin as control were performed for phosphorylated-CAD^{S1859} (n = 2 biological replicates; ** P<0.01 using one-way ANOVA). (**B**) Quantitative RT-PCR assessment of RICTOR mRNA expressions in GSC23 and MES20 GSCs expressing shCONT, shCAD-1, or shCAD-2 (n = 3 independent experiments per group; ** P<0.01 using one-way ANOVA). (**C**) Immunoblot assessment of phosphorylated-CAD^{S1859} levels after treatment with two independent RICTOR shRNA for 48 hours in GSC23 and MES20. Normalized quantifications with Tubulin as control were performed for

phosphorylated-CAD^{S1859} (n = 2 biological replicates; P value was not statistical significant using one-way ANOVA)

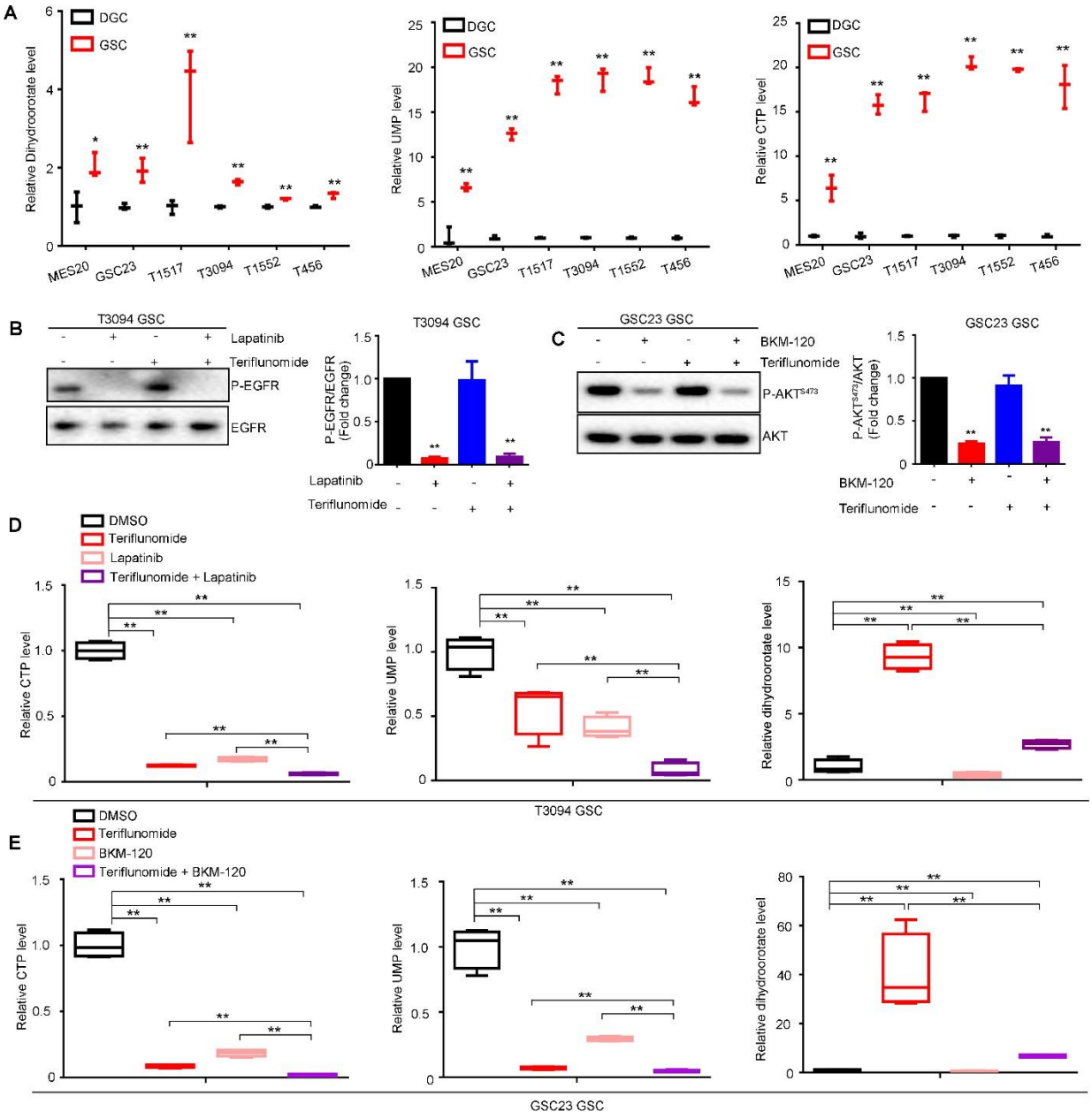

Fig. S12. Combinatorial blockade of de novo pyrimidine synthesis in GSCs by the DHODH inhibitor teriflunomide and EGFR or PI3K inhibition. (**A**) Concentrations of pyrimidine metabolites (dihydroorotate, uridine 5'-monophosphate (UMP), and Cytidine triphosphate (CTP)) were determined using targeted mass spectrometry from cell lysates of GSCs and matched DGCs from six patient-derived glioblastoma specimens (MES20, GSC23, T1517, T3094, T1552, and T456). The relative levels of these

three metabolites were normalized to those of DGCs. Center line represents the median, lower and upper limits of the box represent the 25th and 75th percentiles, and whiskers show maximum and minimum (n = 3 independent experiments per group; ** P<0.01 using two-sided Student's t-test for each pair). (**B**) and (**C**) Immunoblot assessment of phosphorylated-EGFR and phosphorylated-AKT^{S473} after treatment with the EGFR inhibitor (lapatinib) or PI3K inhibitor (LY294002) in combination with DHODH inhibitor (teriflunomide) for 48 hours in T3094 or GSC23 GSCs. Normalized quantifications with Tubulin as control were performed for phosphorylated-EGFR and phosphorylated-AKT^{S473} (n = 3 independent replicates; ** P<0.01 using one-way ANOVA). (**D**) Concentrations of metabolites of pyrimidine synthesis (dihydroorotate, UMP, and CTP) in EGFR-amplified T3094 GSCs treated with four different arms: vehicle control (DMSO), DHODH inhibitor (teriflunomide), EGFR inhibitor (lapatinib), and combined inhibitors (teriflunomide and lapatinib) (n = 4 independent experiments per group; ** P<0.01 using one-way ANOVA). (**E**) Concentrations of metabolites of pyrimidine synthesis (dihydroorotate, UMP, and CTP) in GSC23 GSCs harboring PTEN mutations underwent treatment with four different arms: vehicle control (DMSO), DHODH inhibitor (teriflunomide), PI3K inhibitor (BKM120), and combined inhibitors (teriflunomide and BKM120) (n = 4 independent experiments per group; ** P<0.01 using one-way ANOVA).

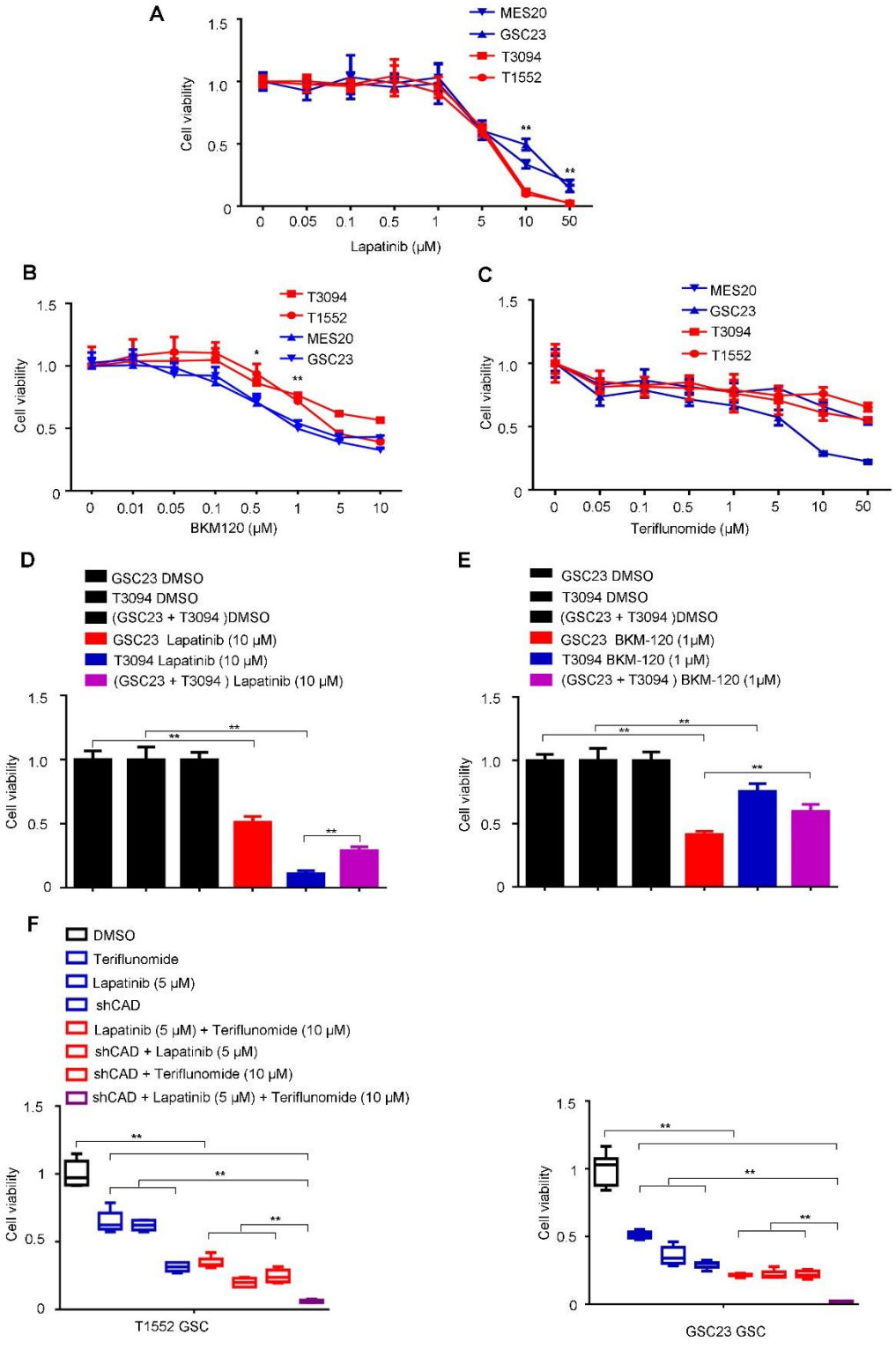

Fig. S13. Sensitivity of GSCs to inhibitor treatments. (**A–C**) Four patient-derived GSCs, two with PTEN deletion without EGFR amplification (GSC23 and MES20, designated in blue) and two with EGFR

amplification with wild-type PTEN (T3094 and T1552, designated in red), were cultured under serum-free conditions and treated with a range of concentrations of a single drug. (**A**) Sensitivity of patient-derived GSCs to the EGFR inhibitor, lapatinib (n = 4 independent experiments per group; ** P< 0.01 using one-way ANOVA). (**B**) Sensitivity of patient-derived GSCs to the PI3K inhibitor, BKM120 (n = 4 independent experiments per group; ** P < 0.01 using one-way ANOVA). (**C**) Sensitivity of patient-derived GSCs to the DHODH inhibitor, teriflunomide (n = 6 independent experiments per group; P value was not statistical significant using one-way ANOVA). (**D**) and (**E**) PTEN deletion (GSC23) and EGFR amplification (T3094) glioma cells were mixed and underwent treatment with BKM120 or lapatinib. Proliferation was measured by CellTiter-Glo (n = 6 independent experiments per group; ** P < 0.01 using one-way ANOVA). (**F**) Growth of T1552 and GSC23 GSCs with triple treatment of BKM120, lapatinib and teriflunomide in comparison to single inhibitor or two inhibitor combination, as measured by CellTiter-Glo (n = 6 independent experiments per group; ** P < 0.01 using one-way ANOVA).

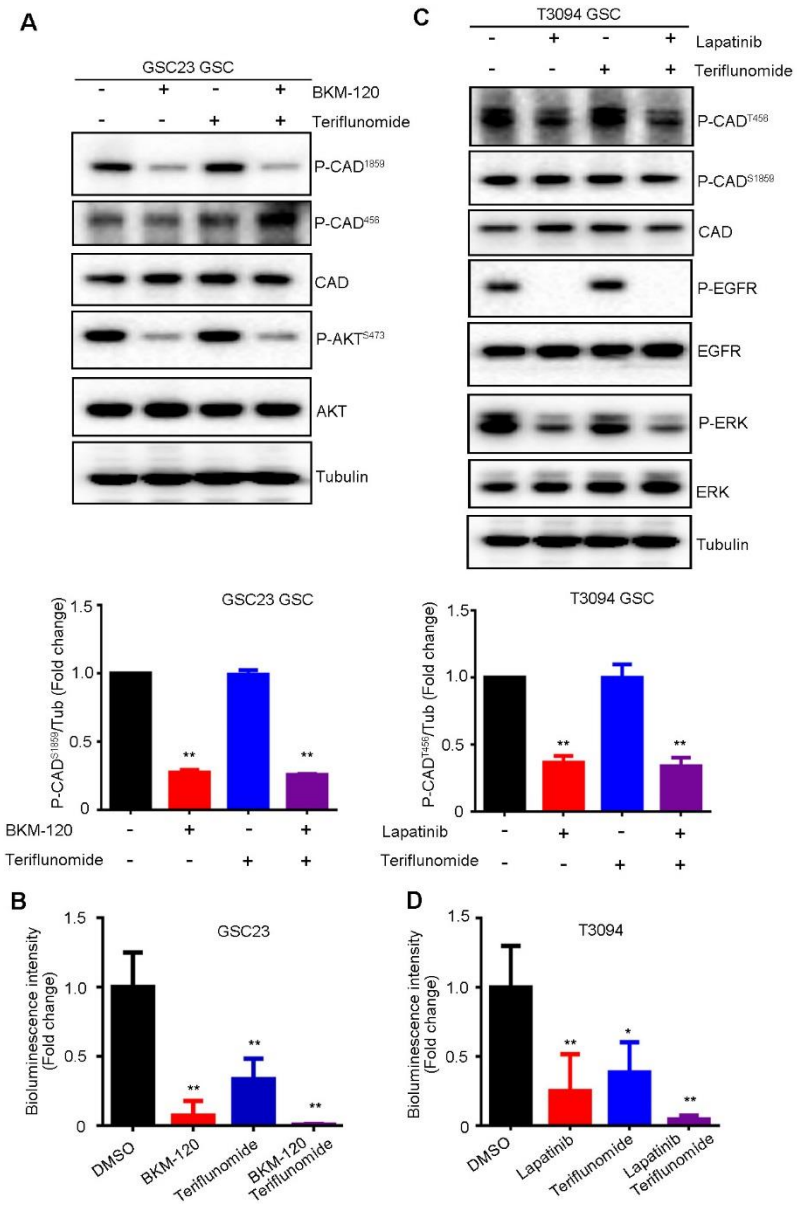

Fig. S14. Impact of targeted therapies on signal transduction pathways in vivo. (**A**) GSC23 cells were implanted into the flanks of immunocompromised mice. Mice bearing established tumors underwent systemic administration of vehicle control, PI3K inhibitor (BKM120), DHODH inhibitor (teriflunomide), or the combination for 20 days. Tumors were harvested and analyzed by immunoblot for phosphorylated-CAD^{S1859}, phosphorylated-CAD^{T456}, total CAD, phosphorylated-AKT, and total AKT protein. Normalized quantifications with Tubulin as control were performed for phosphorylated-CAD^{S1859} (n = 3 independent replicates; ** P<0.01 using one-way ANOVA). (**B**) Quantifications of bioluminescence intensity was

performed for 4 treatment groups from Figure 6A (n = 5 independent experiments per group; ** P<0.01 using one-way ANOVA). (**C**) T3094 GSCs were implanted into the flanks of immunocompromised mice. Mice bearing established tumors underwent systemic administration of vehicle control, EGFR inhibitor (lapatinib), DHODH inhibitor (teriflunomide), or the combination for 20 days. Tumors were harvested and analyzed by immunoblot for phosphorylated-CAD^{S1859}, phosphorylated-CAD^{T456}, total CAD, phosphorylated-EGFR, total EGFR, phosphorylated-ERK, and total ERK protein. Normalized quantifications with Tubulin as control were performed for phosphorylated-CAD^{T456} (n = 3 independent replicates; ** P<0.01 using one-way ANOVA). (**D**) Quantifications of bioluminescence intensity was performed for 4 treatment groups from Figure 6D (n = 6 independent experiments per group; * P < 0.05, ** P < 0.01 using one-way ANOVA).

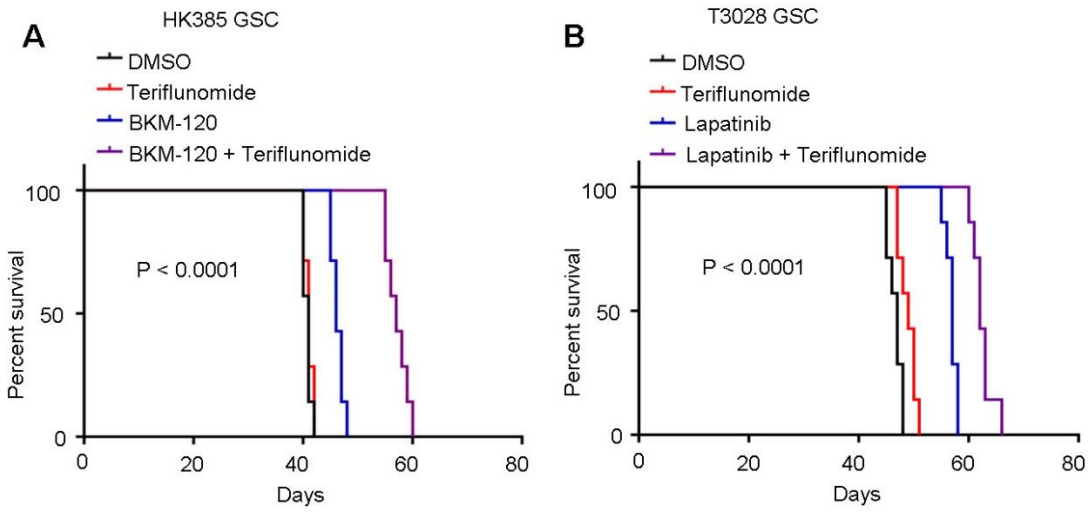

Fig. S15. Combined targeting of pyrimidine synthesis inhibits GSC tumorigenesis in vivo. (**A**) PTEN-deleted HK385 primary GSCs were implanted into the frontal lobes of immunocompromised mice. Tumor-bearing mice underwent treatment with vehicle control, teriflunomide, lapatinib or the combination. Survival is displayed by the Kaplan-Meier method (n = 7 independent experiments per group; ** P < 0.0001 using log-rank test). (**B**) EGFR-amplified T3028 primary GSCs were implanted into the frontal lobes of immunocompromised mice. Tumor-bearing mice underwent treatment with vehicle control, teriflunomide, lapatinib or the combination. Survival is displayed by the Kaplan-Meier method (n = 7 independent experiments per group; ** P< 0.0001 using log-rank test).

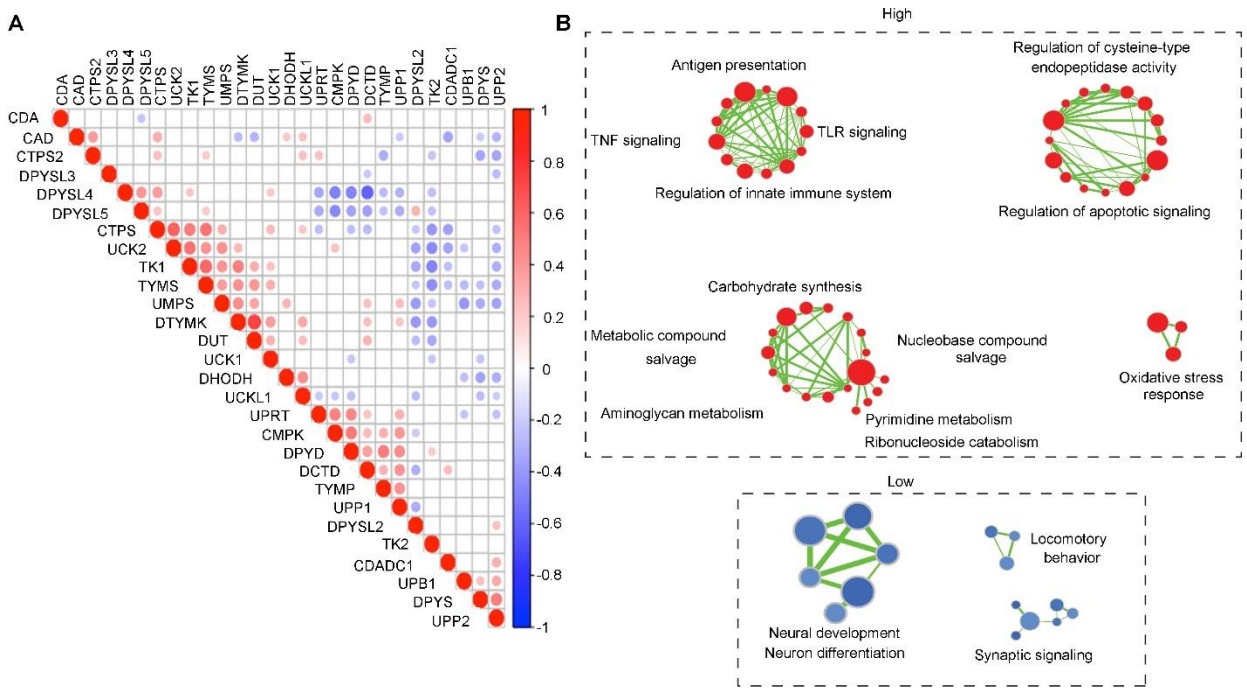

Fig. S16. Pairwise correlation analysis of pyrimidine pathway genes and gene enrichment analysis. (**A**) Correlogram heatmap displaying correlations between mRNA expression levels of 28 genes involved in the pyrimidine biosynthesis pathway. HG-U133A microarray mRNA expression data were derived from patient tumor specimens from the TCGA glioblastoma cohort. (**B**) Gene set enrichment analysis reveals positive correlation of the pyrimidine metabolic signature with regulation of innate immune, apoptotic regulation and metabolism.

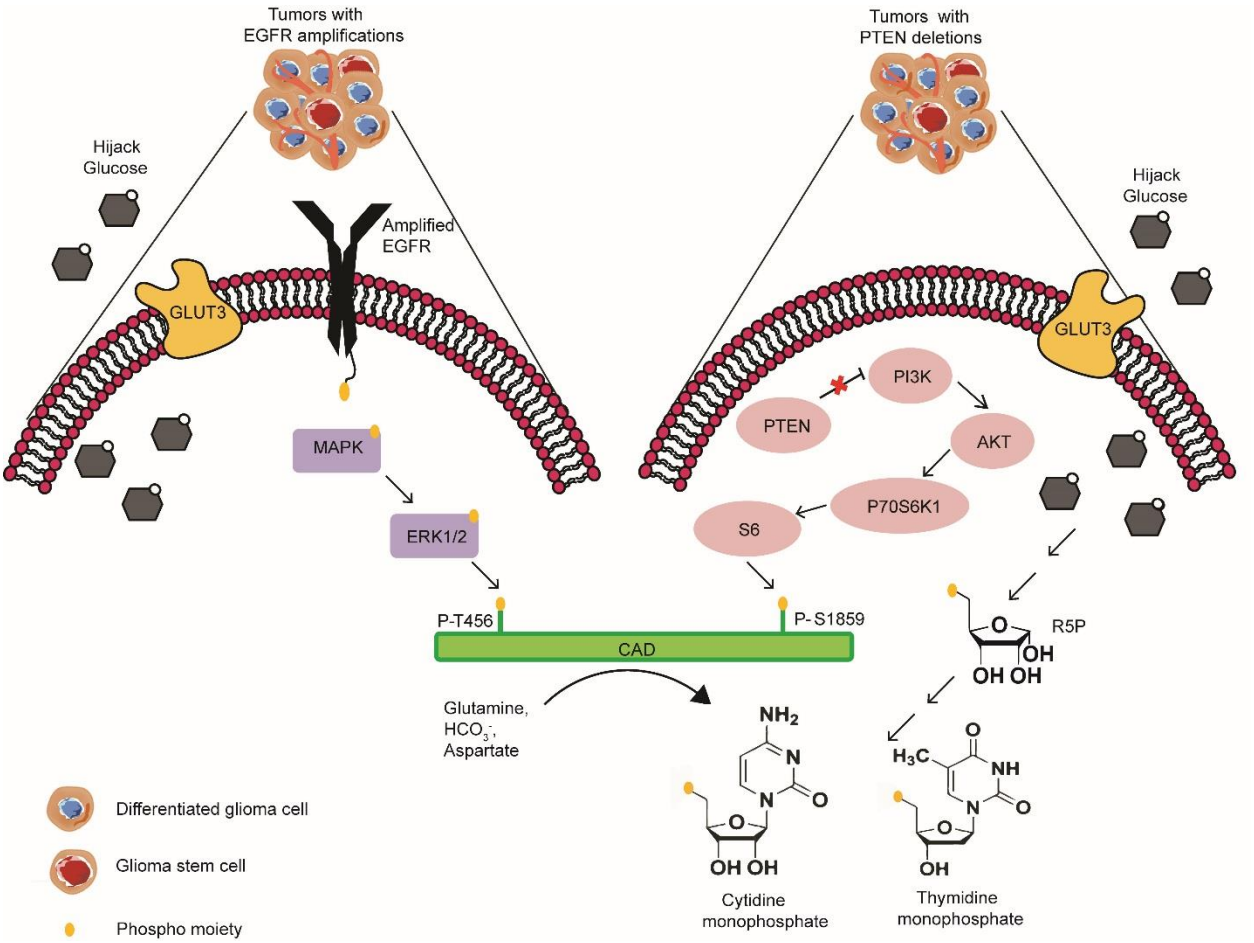

Fig. S17. Proposed model of combined targeting of pyrimidine synthesis in GSCs. Driver mutations of EGFR and PTEN active pyrimidine synthesis through distinct phosphorylation sites on CAD to promote glucose-sustained metabolic reprograming. Therapeutic combination targeting driver mutation and key enzyme in pyrimidine synthesis demonstrated improved inhibition of GSC tumorigenesis.

Data file S1. Individual subject-level data (Excel file).